JBC RESEARCH ARTICLE

Regulation of the activity of the bacterial histidine kinase PleC by the scaffolding protein PodJ

Received for publication, January 28, 2022 Published, Papers in Press, February 3, 2022,
https://doi.org/10.1016/j.jbc.2022.101683

Chao Zhang, Wei Zhao, Samuel W. Duvall, Kimberly A. Kowallis, and W. Seth Childers*

From the Department of Chemistry, University of Pittsburgh, Pittsburgh, Pennsylvania, USA

Edited by Chris Whitfield

Scaffolding proteins can customize the response of signaling networks to support cell development and behaviors. PleC is a bifunctional histidine kinase whose signaling activity coordinates asymmetric cell division to yield a motile swarmer cell and a stalked cell in the gram-negative bacterium *Caulobacter crescentus*. Past studies have shown that PleC's switch in activity from kinase to phosphatase correlates with a change in its subcellular localization pattern from diffuse to localized at the new cell pole. Here we investigated how the bacterial scaffolding protein PodJ regulates the subcellular positioning and activity of PleC. We reconstituted the PleC-PodJ signaling complex through both heterologous expressions in *Escherichia coli* and *in vitro* studies. *In vitro*, PodJ phase separates as a biomolecular condensate that recruits PleC and inhibits its kinase activity. We also constructed an *in vivo* PleC-CcaS chimeric histidine kinase reporter assay and demonstrated using this method that PodJ leverages its intrinsically disordered region to bind to PleC's PAS sensory domain and regulate PleC-CcaS signaling. Regulation of the PleC-CcaS was most robust when PodJ was concentrated at the cell poles and was dependent on the allosteric coupling between PleC-CcaS's PAS sensory domain and its downstream histidine kinase domain. In conclusion, our *in vitro* biochemical studies suggest that PodJ phase separation may be coupled to changes in PleC enzymatic function. We propose that this coupling of phase separation and allosteric regulation may be a generalizable phenomenon among enzymes associated with biomolecular condensates.

Eukaryotic scaffolds add layers of regulation upon signaling pathways that include allosteric mechanisms (1), feedback regulation (2), and phase separation into distinct compartments (3). Scaffold protein phase separation occurs when a protein exhibits weak multivalent interactions with itself or other biomolecules (4). These weak multivalent interactions facilitate the formation of dense and liquid-like droplet assemblies. Given that the assemblies have diameters of hundreds of nanometers to micrometers and recruit and concentrate several proteins, they have also been coined "membraneless organelles" (5). Although phase separation has become a paradigm for spatially organizing biochemistry within eukaryotic cytoplasm (6), examples of phase separation have just recently emerged in bacteria (4, 7). Phase separation has been implicated in organizing a variety of enzymes and biochemical processes in bacteria that include RNA polymerase (8), mRNA decay (9, 10), cell polarity (11, 12), ABC transporters (13), DNA repair (14), cell division (15, 16), chromosome segregation (17), metabolic enzymes associated with day–night cycles (18) and carboxysome assembly (19).

In contrast to eukaryotic scaffolds, the mechanism of how scaffolding proteins impact bacterial signaling pathways has been less studied. Three scaffolds play roles in regulating the subcellular position of histidine kinases involved in the asymmetric cell division of the gram-negative bacterium *Caulobacter crescentus*: PopZ-CckA (20), SpmX-DivJ (21), and PodJ–PleC (22, 23). PopZ (11) and SpmX (12) phase separate as a biomolecular condensate that recruits distinct signaling protein clients (20). At the opposite new cell pole, scaffold PodJ sequesters four distinct signaling proteins directly or indirectly: PleC, PopA, DivL, and CpaE (23). Past *in vivo* fluorescence recovery after photobleaching and single-molecule tracking studies have shown that the new cell pole forms distinct compartments mediated by biomolecular condensates (11, 12, 20). The primary scaffold that phase separates to generate distinct compartments at each cell pole is the scaffold protein PopZ (11, 12, 20). A key question to consider is the roles of proteins at each of the cell pole localized biomolecular condensates. Do other proteins within these *in vivo* biomolecular condensates serve as a scaffold, like PopZ (11), and contribute to phase separation? Or do they serve as clients that do not impact phase separation? Here we examine the *in vitro* phase properties of the PodJ scaffold and consider how it impacts its signaling protein client PleC.

Coordination of *C. crescentus* replication, cell growth, and division requires the bifunctional cell-cycle kinase CckA to undergo a kinase-to-phosphatase switch during each cell cycle (Fig. 1). The activity changes of CckA are facilitated by the bifunctional histidine kinase PleC that also oscillates between kinase and phosphatase activity states (24, 25) (Fig. 1). Several factors contribute to PleC's kinase to phosphatase switch. One factor is that unphosphorylated DivK allosterically stimulates the kinase activity of PleC (26). Second, PleC signaling activity is regulated by pilus retraction upon surface contact (27). In this model, pilus retraction leads to the accumulation of PilA monomers in the periplasm that interacts and regulates PleC

* For correspondence: W. Seth Childers, wschild@pitt.edu.

© 2022 THE AUTHORS. Published by Elsevier Inc on behalf of American Society for Biochemistry and Molecular Biology. This is an open access article under the CC BY license (http://creativecommons.org/licenses/by/4.0/).

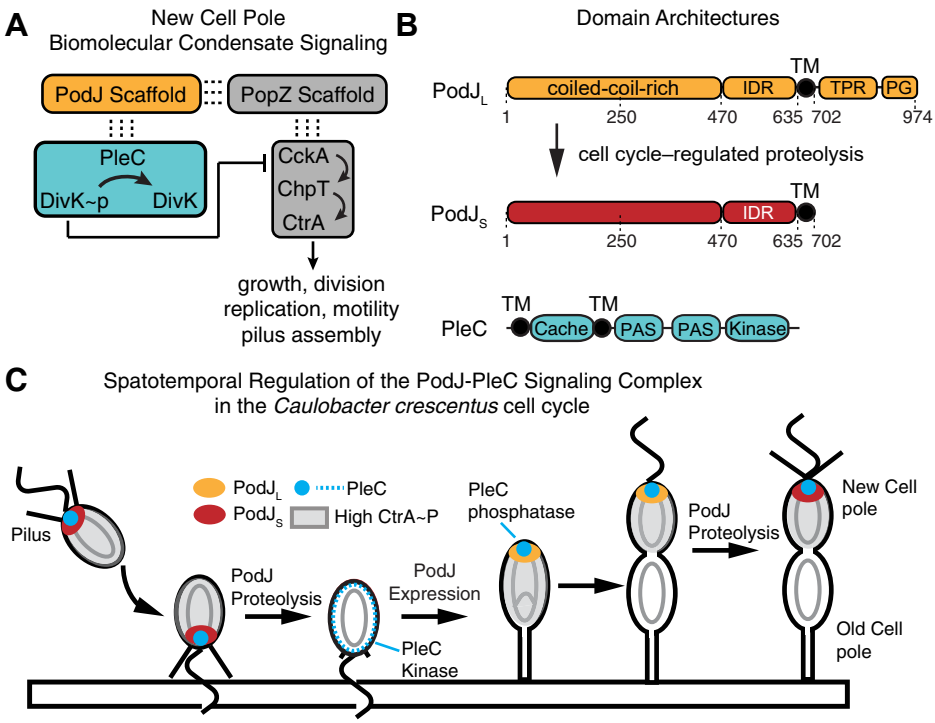

Figure 1. Signaling Pathways organized by a new cell pole localizes biomolecular condensate. *A*, two scaffolding proteins organize signaling proteins within the new cell pole biomolecular condensate: PodJ and PopZ. The ultimate downstream functions of this signaling pathway are more than 90 genes that regulate growth, division, replication, and motility. PopZ (*gray*) recruits the CckA, ChpT, and CtrA signaling protein clients. PodJ (*orange*) directly or indirectly recruits PleC and DivK clients (*cyan*) to the new cell pole. The PleC-DivK two-component system regulates the function of the CckA-ChpT-CtrA phosphorelay. *B*, the domain architecture of $PodJ_L$ and PleC and residue numbers are shown on *top*. *C*, the localization pattern of the PodJ–PleC signaling complex through the *Caulobacter crescentus* cell cycle. $PodJ_L$ (*orange*) expression leads to cell pole accumulation of PodJ–PleC and upregulation of PleC (*blue*) phosphatase function. Proteolysis of PodJ results in a shortened form of PodJ (*red*) that retains cell pole accumulation but does not stimulate PleC phosphatase function. Subsequent proteolysis of PodJ liberates PleC from the cell pole.

activity (27). A third factor that correlates with PleC's activity is its subcellular localization pattern (Fig. 1). When PleC is localized at the new cell pole, it functions as a phosphatase (28). In contrast, when PleC is released from the cell pole in the swarmer-to-stalk transition, PleC functions as a kinase (26).

The cell pole localization pattern of PleC depends on PodJ (22, 29). The PodJ spans the membrane and within the cytoplasm includes six coiled coils, an intrinsically disordered region (IDR) (Figs. 1*B* and S1, *A* and *B*) featured by negatively and positively charged blocks at the N and C termini, respectively, and a transmembrane (TM) anchor. Within the periplasm, PodJ contains a tetratricopeptide repeat domain and a peptidoglycan-binding domain. In *C. crescentus*, deletion of *podJ* results in delocalized PleC and downregulation of the CtrA pathway (23, 29, 30). Moreover, PodJ variants lacking either the cytoplasmic or the periplasmic domains also resulted in downregulation of the CtrA pathway (22) and loss of PleC cell pole localization (30). Thus, both PodJ's cytoplasmic and periplasmic domains contribute to the regulation of CtrA activity (30).

The full-length $PodJ_L$ (full length, 1–974) is expressed in the swarmer to stalk transition (Fig. 1, *B* and *C*). Then upon cell division, full-length $PodJ_L$ is proteolyzed into a shortened form $PodJ_S$ (short form, 1–702) (31, 32), *via* a set of proteases (23, 31, 32). Both $PodJ_L$ and $PodJ_S$ can support cell pole localization of PleC (30). However, the proteolysis of PodJ correlates with the downregulation of the CtrA regulon (30). Therefore, directly or indirectly, the expression and proteolysis of PodJ play a central role in regulating the master regulator CtrA (22, 29).

Here, we applied synthetic biology and *in vitro* biochemical approaches to understand PodJ's role within the new cell pole biomolecular condensate. Our results indicate that PodJ serves as a scaffold that phase separates as a biomolecular condensate *in vitro* that recruits PleC and inhibits PleC kinase activity. Through a complementary synthetic biology strategy, we designed and built a PleC-CcaS chimeric histidine kinase reporter assay that identified domains necessary for the PodJ stimulation of PleC. Our results suggest a model in which PodJ phase separates as a biomolecular condensate that recruits and regulates PleC signaling activity.

Results

PodJ coiled coils contribute to cell pole localization

To understand how PodJ impacts PleC's function, we reconstituted the PodJ–PleC signaling complex in *Escherichia coli*. Past studies have shown that heterologous expression of PodJ in *E. coli* resulted in cell pole accumulation (20). Of note, the gamma-proteobacterium *E. coli* is divergent from the alphaproteobacterium *C. crescentus* and does not contain any *C. crescentus* polarity protein homologs (33). Therefore, *E. coli*

has been used extensively as a heterologous system for testing *C. crescentus* protein–protein interactions (20, 34).

Previous studies have also shown that an N-terminal YFP fusion to PodJ does not disrupt its regulation of the CtrA pathway in *C. crescentus* (29). Therefore, to reconstitute the PodJ–PleC complex, we heterologously expressed an N-terminal fluorescent fusion protein of PodJ(YFP-PodJ) in *E. coli* and determined its subcellular localization pattern. As shown in Fig. S2*A*, YFP-PodJ accumulated at the cell poles. We also found that PodJ variants lacking the periplasmic domains, transmembrane tether, IDR, or coiled coil 4 to 6 (CC4–6) also accumulated at the cell poles. In contrast, PodJ variants lacking coiled coil 1 to 3 (CC1–3) did not accumulate at the cell poles in *E. coli* (Fig. S2*A*).

In *C. crescentus*, Lawler *et al.* (30) observed that both the cytoplasmic and the periplasmic domains alone of PodJ could accumulate at the cell poles. Therefore, PodJ has at least two independent mechanisms for localizing to the cell poles. We, therefore, interrogated the role of CC1–3 in the subcellular localization of PodJ's cytoplasmic domains, YFP-PodJ(1–635). As in *E. coli*, we observed that YFP-PodJ(1–635) accumulated at the cell poles in *C. crescentus* (Fig. 2*A*). In contrast, we observed that sfGFP-PodJ(250–635) was diffuse or patchy when expressed as a sole copy in *C. crescentus* (Fig. 2*A*). This suggests that CC1–3 is critical for the ability of PodJ's cytoplasmic domains to accumulate at the cell poles.

PleC localizes to the cell pole via *PodJ's IDR*

With an understanding of the domains that contribute to PodJ subcellular localization (Figs. 2*A* and S2*A*), we then interrogated if YFP-PodJ recruits PleC-mCherry to the cell poles in *E. coli*. The expression of PleC alone resulted in a diffuse localization pattern (Fig. S2*A*). In contrast, coexpression of PodJ and PleC resulted in colocalization at the cell poles in 98% of cells. To interrogate the interaction between YFP-PodJ and PleC-mCherry, we heterologously coexpressed full-length PleC-mCherry with a library of YFP-PodJ domain deletion variants in *E. coli* (Fig. S2*A*). Deletion of the periplasmic domains, the TM or CC4–6, did not affect the cell pole localization of YFP-PodJ or PleC-mCherry recruitment to the cell poles. In contrast, the YFP-PodJΔIDR variant was unable to recruit PleC-mCherry to the cell poles (Fig. S2*A*).

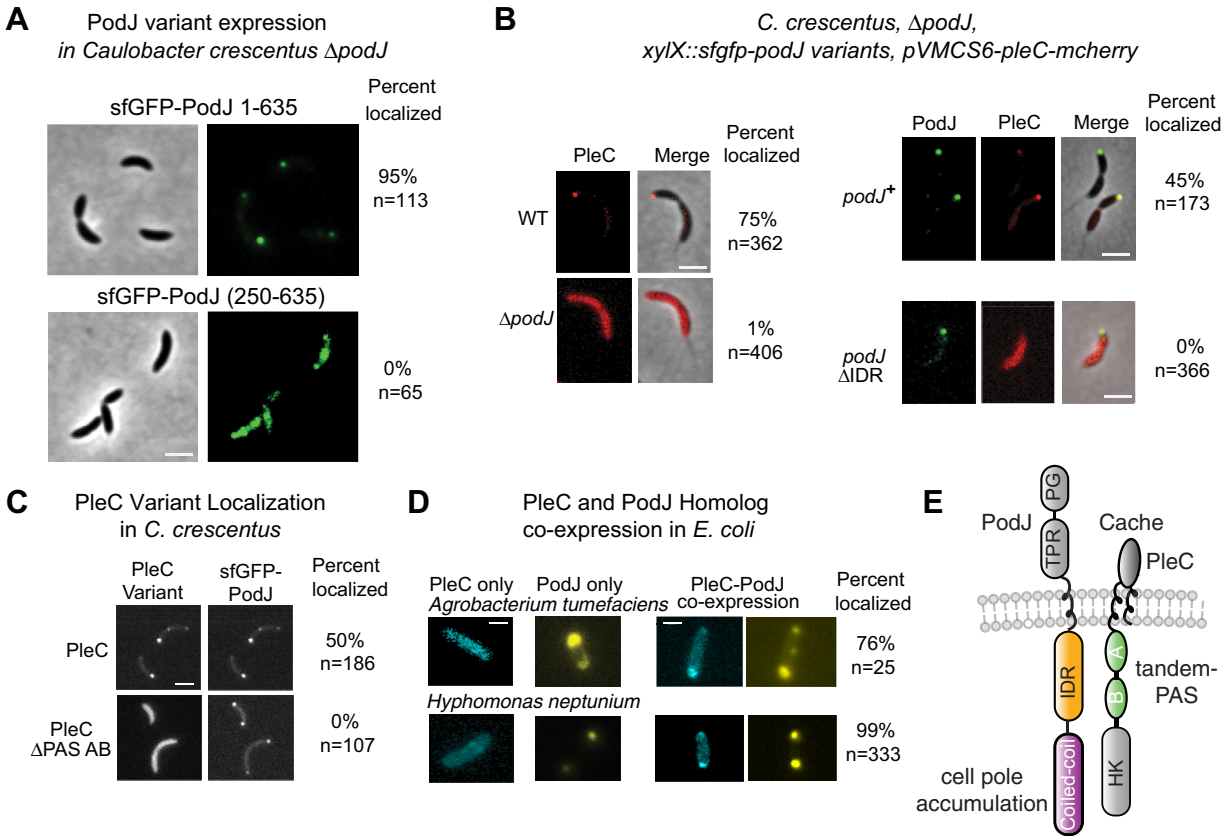

Figure 2. Identification of PodJ and PleC domains critical for colocalization at the cell pole. *A*, expression of sfGFP-PodJ(250–635) and sfGFP-PodJ(1–635) as a sole copy in *podJ* deletion *C. crescentus* strain. The scale bar represents 2 μm. *B*, expression of PleC-mCherry in wildtype *C. crescentus*, the *podJ* deletion strain, and the *podJ* deletion strain supplemented full-length sfGFP-PodJ or sfGFP-PodJ-ΔIDR and their localization analysis. The scale bar represents 2 μm. Strains were cultured into mid-log phase and induced with 0.03% xylose for sfGFP-PodJ and 0.05 mM vanillic acid for PleC-mCherry for 5 h before imaging. *C*, localization of PleC-mCherry or PleCΔPAS-AB with sfGFP-PodJ in the *C. crescentus podJ-pleC* deletion strain. Strains were cultured into the mid-log phase and induced with 0.5 mM vanillic acid for PleC-mCherry for 3 h before imaging. The scale bar represents 2 μm. For each image, the percent colocalized and the number of cells analyzed are reported. *D*, YFP-PodJ and PleC-CFP pairs from other alphaproteobacteria species colocalize at the cell poles when coexpressed in *E. coli*. YFP-PodJ was induced with 0.5 mM IPTG, and PleC-mCherry was induced with 1 mM arabinose for 2 h. The scale bar represents 2 μm. *E*, annotation of PodJ and PleC functions indicates an IDR-PAS protein–protein interaction and that PodJ's N-terminal coiled coils are critical for cell pole accumulation. For simplicity of illustration, PleC naturally exists as a dimer but is depicted as a monomer.

This suggests that PodJ's IDR may be a site of interaction with PleC-mCherry in *E. coli*.

We next tested if PodJ's IDR was critical for PleC localization in *C. crescentus* (Fig. 2*B*). Past work has shown that PleC-GFP localized at the new cell pole in predivisional cells (28) and was dependent on PodJ (30). Consistent with these findings, we observed that, in a *podJ* deletion background, PleC-mCherry exhibited a diffuse localization pattern (Fig. 2*B*). Expression of sfGFP-PodJΔIDR accumulated at the cell poles in *C. crescentus* (Fig. 2*B*). However, sfGFP-PodJΔIDR was unable to recruit PleC-mCherry to the cell poles (Fig. 2*B*). Our observation is consistent with previous PodJ domain analysis in *C. crescentus* (30) which indicated that a portion of the IDR of PodJ contributes to PleC's new cell pole localization in *C. crescentus* (23, 30). Therefore, PodJ serves as a scaffold that recruits PleC as a client through its IDR.

PleC localizes at the cell pole via *its tandem PAS sensor*

We next asked which domains within PleC serve as the site of interaction with PodJ. PleC contains a periplasmic Cache domain, two cytoplasmic PAS domains in tandem, and a histidine kinase domain. Thus, we heterologously expressed a set of PleC-mCherry domain deletion variants and YFP-PodJ in *E. coli* (Fig. S2*B*). We observed that PleC-mCherry variants that lack the periplasmic Cache domain or the HK domains colocalized with YFP-PodJ. In contrast, PleCΔPAS-AB-mCherry displayed a diffuse localization pattern. This suggests that PleC's PAS-AB is required for recruitment to the cell pole by PodJ in *E. coli*.

To corroborate the importance of PAS-AB, we examined the subcellular localization of PleCΔPAS-AB-mCherry or PleC-mCherry in a *podJ* and *pleC* deletion *C. crescentus* background. We observed that the PodJ–PleC complex colocalized in predivisional cells at the new cell pole (Fig. 2*C*). In contrast, in *C. crescentus* strains expressing sfGFP-PodJ and PleCΔPAS-AB-mCherry, the PleC variant displayed a diffuse subcellular localization pattern. This suggests that the PleC-PAS-AB: PodJ-IDR protein–protein interaction is also critical for PleC recruitment to the cell pole in *C. crescentus*.

To determine if the PodJ–PleC interaction is conserved across alphaproteobacteria that encode both PleC and PodJ, we heterologously expressed PodJ and PleC homologs from *Agrobacterium tumefaciens* (Atu) and *Hyphomonas neptunium* (Hyp) individually and together in *E. coli* (Fig. 2*D*). Both YFP-AtuPodJ and YFP-HypPodJ accumulated at the cell poles in *E. coli*, while heterologous expression of AtuPleC-CFP or HypPleC-CFP individually resulted in a diffuse localization pattern. However, each PodJ homolog colocalized with its cognate PleC at the cell pole (Fig. 2*D*) upon coexpression. Therefore, the ability of PleC and PodJ to colocalize at the cell poles in *E. coli* is conserved among these species. Within a representative set of 11 alphaproteobacterial species, we found that the presence of *pleC's* cytoplasmic PAS-A and PAS-B sensory domains correlates with the existence of *podJ* and *pilA* homologs in the genome (Fig. S3). This coconservation agrees with the requirement of PAS-AB for PleC's recruitment to the cell poles (Figs. 2, *D* and *E* and S2*B*).

In addition, we found that each of the studied PodJ homologs contains a putative IDR (Fig. S4). These IDRs vary in length from 242 to 261 residues and are flanked by coiled coil–rich regions (Fig. S4*A*). Although the sequences of the IDR are nonconserved, each IDR is composed of two distinct regions (Fig. S4*B*). One IDR region is rich in negative charges with pI (isoelectric point) between 3.4 and 3.9. In contrast, an adjacent IDR within each PodJ homolog is rich in positive charges with pIs between 9.9 and 10.9. This conservation of charge pattern within the IDRs may play a role in PodJ function.

Design of a PleC-CcaS chimeric histidine kinase

Owing to PodJ interacting with the PleC's sensory domains (Figs. 2 and S2), we hypothesized that PodJ might also regulate PleC function. Complete reconstitution of the PleC signaling network would require the addition of PodJ, PleC, DivK, DivL, CckA, ChpT, CtrA, and a CtrA regulated promoter. We, therefore, leveraged the demonstrated technique of exchanging kinase sensory domains to construct a chimeric histidine kinase to simplify our approach (35, 36). We applied this approach using the green light–sensing CcaS-CcaR system (37) to interrogate the responsiveness of PleC's sensor to PodJ expression.

We designed, built, and tested a PleC-CcaS chimeric histidine kinase library (Fig. S5). Each variant consisted of PleC's tandem PAS sensor fused to different junction sites within the histidine kinase domain of CcaS (Figs. S3, *A* and *B* and S5*A*). The *pleC-ccaS* chimera was coexpressed with its cognate response regulator *ccaR*. Upon phosphorylation, phosphor-CcaR activates transcription of *mCherry* from the *cpcG2* promoter (Fig. 3*B*). We found that the YFP-PleC-CcaS retained its ability to colocalize with CFP-PodJ in *E. coli* (Fig. 3*C*). In the absence of PodJ stimulation, the PleC-CcaS chimera exhibited little mCherry expression. In comparison, mCherry expression was highest using chimera AB-1 upon coexpression with PodJ (Fig. S5*B*). Therefore, the engineered PleC-CcaS chimera retains the on-switch function (Fig. 3*D*) of the parent green light–sensing CcaS (37). The PleC-CcaS chimera AB-1 connects PAS-AB to CcaS between the D and V of the conserved DVT hinge motif (38) (Fig. S6, *A*–*C*). These results suggest that we have engineered a functional PodJ-responsive PleC-CcaS chimeric histidine kinase.

Stimulation of PleC-CcaS activity requires PodJ's IDR

To determine whether PleC-CcaS stimulation depended upon specific interactions with PodJ, we compared the effects of coexpressing the YFP-PodJ domain deletion variants with the PleC-CcaS chimera (Fig. 3*D*). Before the analysis, we confirmed that the YFP-PodJ variant displayed fluorescence over 10-fold greater than the empty vector (Fig. S7*A*). Relative to the empty vector control, the expression of PodJ stimulated the PleC-CcaS chimera and resulted in a 10-fold increase in mCherry expression (Fig. 3*D*). However, a PodJ variant that lacks the IDR, YFP-PodJ-ΔIDR, was unable to stimulate PleC-CcaS-mediated mCherry expression. In contrast, expression of the YFP-IDR alone led to a 3-fold activation of mCherry

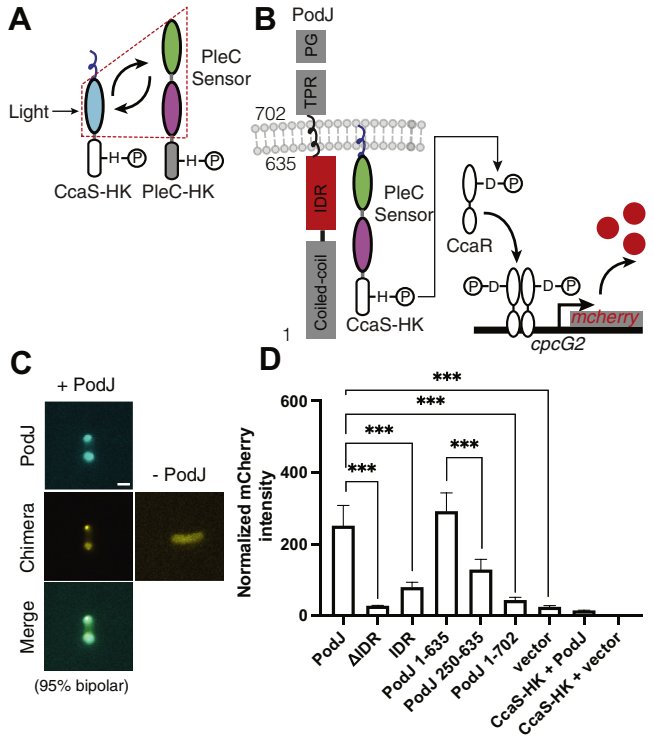

Figure 3. PodJ stimulates the kinase activity of the PodJ-CcaS chimeric histidine kinase in *E. coli*. *A*, design of a PleC-CcaS chimera reporter system. PleC's cytoplasmic sensory domains were fused to the histidine kinase domain of CcaS. The LOV domain was swapped with PleC's PAS-AB domain to create a PleC-CcaS chimeric histidine kinase. *B*, upon interaction with PodJ, the PleC-CcaS chimeric histidine kinase phosphorylates CcaR, which then stimulates the expression of mCherry *via* binding to the *cpcG2* promotor. *C*, heterologous coexpression of CFP-PodJ together with YFP-PleC-CcaS in *E. coli*. CFP-PodJ was induced with 0.5 mM IPTG for 3 h, and PleC-CcaS-YFP was constitutively expressed. The scale bar represents 2 μm. *D*, coexpression of the PleC-CcaS chimera gene reporter system together with PodJ variants. A two-tailed *t* test was performed. (n.s: $p > 0.05$, $^{*}p \leq 0.05$, $^{**}p \leq 0.01$, $^{***}p \leq 0.001$). Error bars represent the standard deviation from three independent biological replicates performed on different days.

expression (Fig. 3*D*). This suggests that stimulation of the PleC-CcaS chimera is dependent upon the interaction with PodJ's IDR. However, full stimulation of PleC-CcaS requires the entire cytoplasmic domain, suggesting a role of the coiled coils in PleC-CcaS regulation.

PodJ$_S$ is unable to stimulate the PleC-CcaS chimera

Next, we asked if the PleC-CcaS chimera could be stimulated by PodJ$_S$, the primary form in *C. crescentus* swarmer cells. Past experiments indicated that loss of the periplasmic domain leads to reduced expression of CtrA-mediated genes in *C. crescentus* (23). We observed that PodJ$_L$ and PodJ$_S$ could recruit PleC to the cell poles when heterologously expressed in *E. coli* (Fig. S2*A*), consistent with the past observation in *C. crescentus* (22). Therefore, the downregulation of the CtrA pathway upon PodJ proteolysis is not due to a loss of PleC-PodJ binding. Unlike the expression of full-length PodJ$_L$ we observed that expression of PodJ$_S$ was unable to stimulate mCherry expression *via* the PleC-CcaS chimera (Fig. 3*D*).

The loss of PodJ$_S$ stimulation of PleC could result from an altered PodJ transmembrane anchoring that allosterically affects the IDR-PAS conformational state. Therefore, we also examined if PodJ variants lacking the TM tether (PodJ(1–635)) could relieve steric effects on the IDR-PAS conformation. We observed that the cytoplasmic PodJ variant lacking the TM tether stimulated mCherry expression in the PleC-CcaS reporter assay (Fig. 3*D*). This indicates that PodJ's cytoplasmic domains alone can stimulate PleC-CcaS function. Meanwhile, it suggests that the transmembrane region may regulate the PodJ–PleC signaling complex, consistent with the reduced CtrA pathway activation of strains expressing PodJ$_S$ in *C. crescentus* (23, 30).

We next asked how cell pole accumulation of the PodJ–PleC complex impacted PleC-CcaS signaling. The construct lacking the N-terminal coiled coils, PodJ(250–635), does not accumulate at the cell poles in *E. coli* (Fig. S2) or *C. crescentus* (Fig. S1). We found that PodJ(250–635) led to a 3-fold increase in mCherry expression compared with PodJ(1–635), which stimulated a 10-fold increase. These results indicate that cell pole accumulation of PodJ is not required for PleC-CcaS stimulation but may impact the degree of PleC-CcaS stimulation.

Stimulation of PleC-CcaS requires functional PAS domains

Given that PodJ recruits PleC through its cytoplasmic tandem PAS sensory domains, we hypothesized that the regulation of PleC-CcaS kinase domains requires sensory domain stimulation. Our sequence analysis indicated that PleC's PAS A and B domains share low similarities (47.88%) (Fig. S6*A*). In contrast, PAS-A homologs across alphaproteobacteria exhibit 68.3% sequence similarity, whereas PAS-B homologs exhibit 64.4% (Fig. S6*D*). Therefore, we suspect that each PAS domain may have a distinct function.

Previous studies have shown that the signal transmission motif D-I/V-T at the C terminus of the PAS domain allosterically relays signals from the central binding cavity to the C-terminal coiled-coil linker (39). These studies showed that mutations of the Asp to Ala or the Thr to Ala within this motif disrupted the PAS sensor's sensitivity to signal stimulation (36, 38). Similarly, we hypothesized that PodJ's stimulation of PleC activity also requires PleC's PAS-A and PAS-B conserved motifs (39) (Fig. S6).

We, therefore, generated PAS-A (D433A, V435A) and PAS-B (D548A, V550A) hinge motif PleC-CcaS variants to disrupt signal flow within each PAS domain (Fig. 4*A*). Before analysis, we confirmed the expression of PodJ by measuring the fluorescence intensity of N-terminal YFP (Fig. S7*B*). The wildtype PleC-CcaS chimera displayed a 10-fold increase in mCherry expression upon PodJ induction. In contrast, PleC-CcaS PAS-A and PAS-B variants showed little to no stimulation by the expression of PodJ$_L$ (Fig. 4*B*). Also, compared with wildtype, the changes to the PAS domain motif appear to lock the downstream kinase into a state with a low activity, which was insensitive to PodJ expression. Thus, the reduction of stimulation by PodJ could be due to a loss of PAS domain allostery or loss of PodJ–PleC colocalization. Moreover, each PAS domain should be functional to mediate PodJ stimulation of PleC-CcaS.

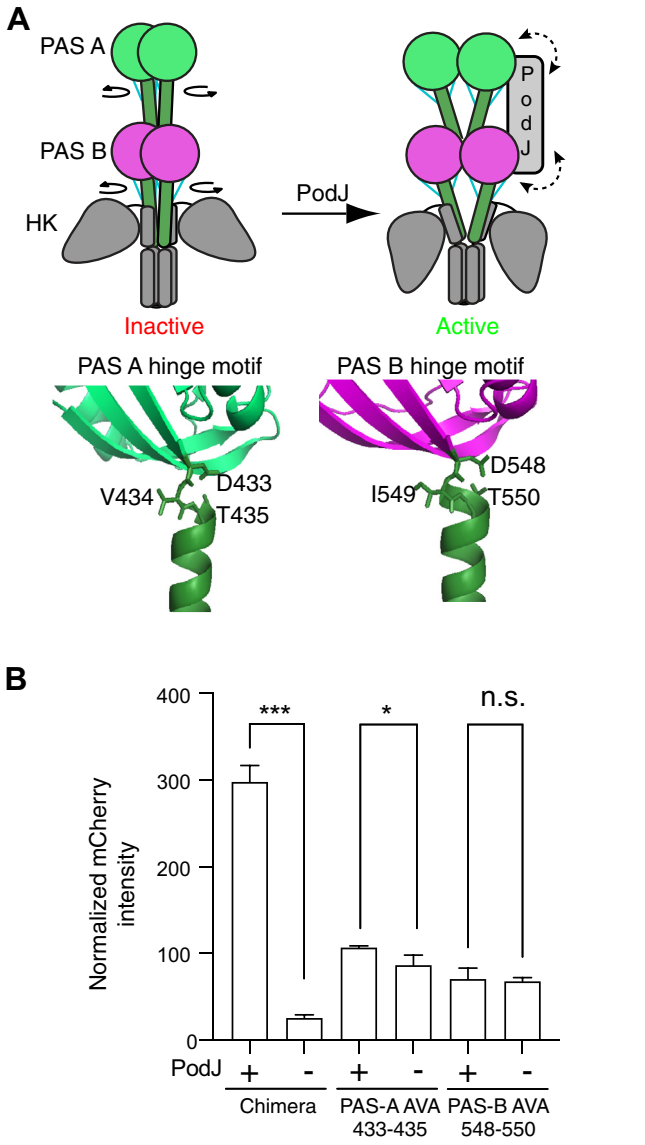

Figure 4. Stimulation of the PleC-CcaS chimera by PodJ depends on the signaling transmission motifs at the C terminus of PleC PAS-A and PAS-B. *A*, cartoon of the conformational change that occurs at the signal transmission motif of sensor kinases. The signal transmission motifs between PAS-A (*green*), PAS-B (*magenta*), and the coiled-coil linker (*green*) contain residues that form several hydrogen bonds (*blue*) and serve as a conformational switch. Homology model of PleC compared with YF1 (PDB ID: 4GCZ-A) (38). In the *left cartoon*, a *curled arrow* around the end of each PAS domain indicates the relative rotation of the N-terminal linker upon signal stimulation. The bidirectional *dashed arrow* in the *right cartoon* suggests the interaction between PodJ and PleC PAS sensory domains. *B*, mutation of the PAS-A (D132A, T134A) or PAS-B (D247A, T249A) PAS sensor transmission motif results in PleC-CcaS mutant chimeras that are unresponsive to $PodJ_L$. Error bars represent the result of three independent biological replicates. A two-tailed *t* test was performed. (n.s: $p > 0.05$, *$p \leq 0.05$, **: $p \leq 0.01$, ***: $p \leq 0.001$)

PodJ forms biomolecular condensates in vitro

To reconstitute the PodJ–PleC signaling system *in vitro*, we utilized PodJ(1–635) as it accumulated at the cell poles (Figs. 2*A* and S2*A*) and stimulated PleC-CcaS signaling (Fig. 3*D*). By size exclusion chromatography and native gel analysis, we observed that PodJ oligomerized as a high-molecular-weight oligomer (>670 kDa) (Fig. 5, *A* and *B*). This large oligomer size could be poised to mediate weak multivalent interactions that promote phase separation. Indeed, we observed *in vitro* that the sfGFP-PodJ(1–635) protein phase separates as round protein-rich droplets with a saturation concentration between 1.5 and 2.0 μM (Figs. 5*C* and S8*A*). This C_{sat} is less than the estimated PodJ concentration in cells from ribosome profiling measurements of 2 to 5 μM (40). Moreover, time-lapse imaging revealed that the PodJ droplets fuse upon contact and gradually relax back to a spherical droplet over 12 min, demonstrating liquid-like properties *in vitro* (Fig. 5*D*).

To determine the impact of fluorescent protein interactions, we observed that sfGFP did not form any visible droplets (Figs. 5*C* and S8*B*). In addition, SNAP-tag fused to the N-terminal PodJ(1–635) also formed droplets at the same condition with a smaller size (Fig. S8*C*). These results indicate that PodJ's droplet formation does not require sfGFP. However, weak fluorescent protein interactions likely mediate increases in protein droplet size.

To interrogate the biomolecular condensate material properties of PodJ, we examined the impact of 1,6-hexanediol, which is commonly used to disrupt weak hydrophobic interactions and dissolve biomolecular condensates (41). We observed that the addition of 10% 1,6-hexanediol disrupted droplet formation (Fig. S9*A*). Moreover, high concentrations of adenosine triphosphate (ATP) have been shown to suppress liquid–liquid phase separation assemblies through the interaction of ATP with hydrophobic or aromatic side chains that attenuate multivalent interactions of phase separating proteins (12, 42, 43). Similarly, we observed that the addition of 10 to 20 mM ATP or ADP led to a reduction in droplet size, partitioning ratio, and PleC-mCherry recruitment (Fig. S9, *B* and *C*). In contrast, we observed that the addition of physiological concentrations of 125 to 1000 μM ATP led to increased sfGFP-PodJ droplet size and partitioning (Fig. S9, *B* and *D*). This increase in droplet size and partitioning may suggest ATP binding to PleC, and subsequent biochemical activities may influence droplet size. In summary, the PodJ biomolecular condensate assembly properties are tunable by adding common small-molecule liquid–liquid phase separation regulators.

We next considered if the ability to localize at the cell poles correlated with PodJ's ability to phase separate *in vitro*. Therefore, we purified and analyzed sfGFP-PodJ(250–635), which lacks CC1–3 (Fig. 5*C*). We observed that sfGFP-PodJ(250–635) increased the critical assembly concentration to between 3.5 and 4.0 μM (Figs. 5*C* and S8*A*) and about 2-fold higher than sfGFP-PodJ(1–635). Therefore, the N-terminal coiled-coil domains are needed for robust PodJ phase separation *in vitro* (Figs. 5*C* and S8*A*) and mediate PodJ cell pole accumulation *in vivo* (Fig. 2*A*).

PodJ biomolecular condensate recruits PleC in vitro

We then considered if the *in vitro* sfGFP-PodJ(1–635) biomolecular condensates could recruit PleC-mCherry as a client. We observed that PleC-mCherry could readily accumulate within the PodJ-rich droplets, whereas mCherry alone was not enriched (Fig. 6*A*). In contrast, mCherry, mCherry + sfGFP,

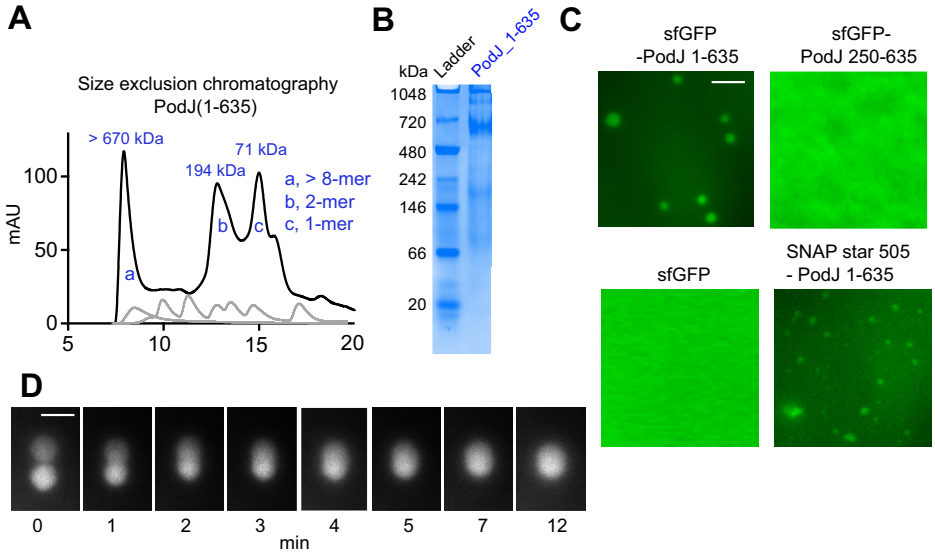

Figure 5. PodJ phase separates as a biomolecular condensate *in vitro*. The oligomerization state of PodJ(1–635) was analyzed *via* (*A*) size exclusion chromatography and (*B*) native gel. *C*, fluorescence microscopy images of purified sfGFP-PodJ(1–635), sfGFP-PodJ(250–635), sfGFP, and SNAP-PodJ(1–635) at 7.5 μM, 50 mM Tris-HCl pH 8.0 and 200 mM KCl. The scale bar represents 5 μm. Concentration-dependent assembly of each construct is reported in Fig. S8. *D*, time-lapse imaging of individual PodJ droplets undergoing dynamic liquid-like fusion events. The scale bar represents 5 μm.

PleC PAS AB-HK-mCherry, and mCherry + sfGFP-PodJ 1–635 did not form droplets under the same condition (Fig. S8*B*).

We employed an *in vitro* fluorescence polarization assay to detect the interaction between PodJ's IDR and histidine kinases colocalized with PodJ at the new cell pole, including PleC PAS-AB domains, DivL, and CckA. We fluorescently labeled PodJ's IDR with a BODIPY dye and observed robust binding between PleC and PodJ's IDR. In contrast, we could not detect any interactions between PodJ's IDR and DivL and CckA (Fig. 6*B*). These fluorescence polarization studies indicate that PleC's tandem PAS domains interact specifically with the IDR from PodJ.

PodJ represses PleC kinase activity in vitro

To evaluate the impact of PodJ(1–635) upon PleC, we employed a coupled enzyme assay to detect changes in kinase activity (44). PleC PAS AB-HK at 7.5 μM supplemented with 1000 μM ATP displayed a 2×10^{-8} M s^{-1} ADP production rate (Fig. 6*C*). We observed dose-dependent repression of the ADP production rate upon addition of PodJ(1–635) to PleC PAS AB-HK. We also found that the addition of 2.5 μM PodJ(1–635) to PleC PAS AB-HK at 7.5 μM supplemented with 1000 μM ATP displayed a 1.1×10^{-9} M s^{-1} ADP production rate with an IC_{50} of 1.86 ± 0.07 μM.

We next asked if the diminished phase separation capabilities of PodJ(250–635) impact its catalytic capabilities. We observed that the ADP production IC_{50} for PodJ(250–635) was 2-fold higher than that for PodJ(1–635). Interesting, our imaging of sfGFP-PodJ(1–635) or sfGFP(250–635) indicated that low concentrations of PodJ protein do not phase separate and do not repress PleC kinase activity. In contrast, higher PodJ concentrations of both constructs led to phase separation and repression of PleC kinase activity (Fig. 6*D*). However, the addition of bovine serum albumin (BSA) resulted in no change in PleC ATP hydrolysis activity (Fig. 6*C*). Therefore, the interaction of PodJ with PleC specifically represses PleC's histidine kinase function. Although kinase activity repression typically correlates with increased phosphatase function (24, 45, 46), future biochemical studies should examine how PodJ impacts PleC's ATP binding, phosphatase, and phosphotransfer functions.

In vivo, PleC-CcaS chimera is inactive when expressed alone, and the addition of PodJ(1–635) stimulated kinase activity (Fig. 3*D*). By contrast, *in vitro*, PleC exhibited kinase activity in solution alone, but the addition of PodJ(1–635) represses PleC kinase activity (Fig. 6*C*). The differences in regulation are likely rooted in aspects of the PleC-CcaS design and the regulatory behavior of the CcaS histidine kinase. Of note, the two-parent kinases PleC and CcaS diverge in structure and regulatory mechanisms. The PodJ sensing PleC functions as an OFF switch, whereas the green light–sensing CcaS functions as an ON switch. Here we observed that the PleC-CcaS chimeric histidine kinase adopts the same ON-switch behavior as the parent CcaS histidine kinase.

In addition, past structure–function studies of PAS-linked histidine kinases have shown that alterations of the N or C terminus of PAS sensory domains can impact sensor functions as an ON switch or as an OFF switch upon signal stimulation (38, 47). Other studies have also shown that the linker length between the sensory domain of CcaS and the HK can alter kinase signaling from an OFF to an ON state (48). Therefore, based on these past studies, the same modifications to PleC-CcaS *versus* PleC can also influence ON-switch *versus* OFF-switch histidine kinase function. Nevertheless, both experimental sets provide evidence that PleC's tandem sensory domain serves as a sensor for PodJ.

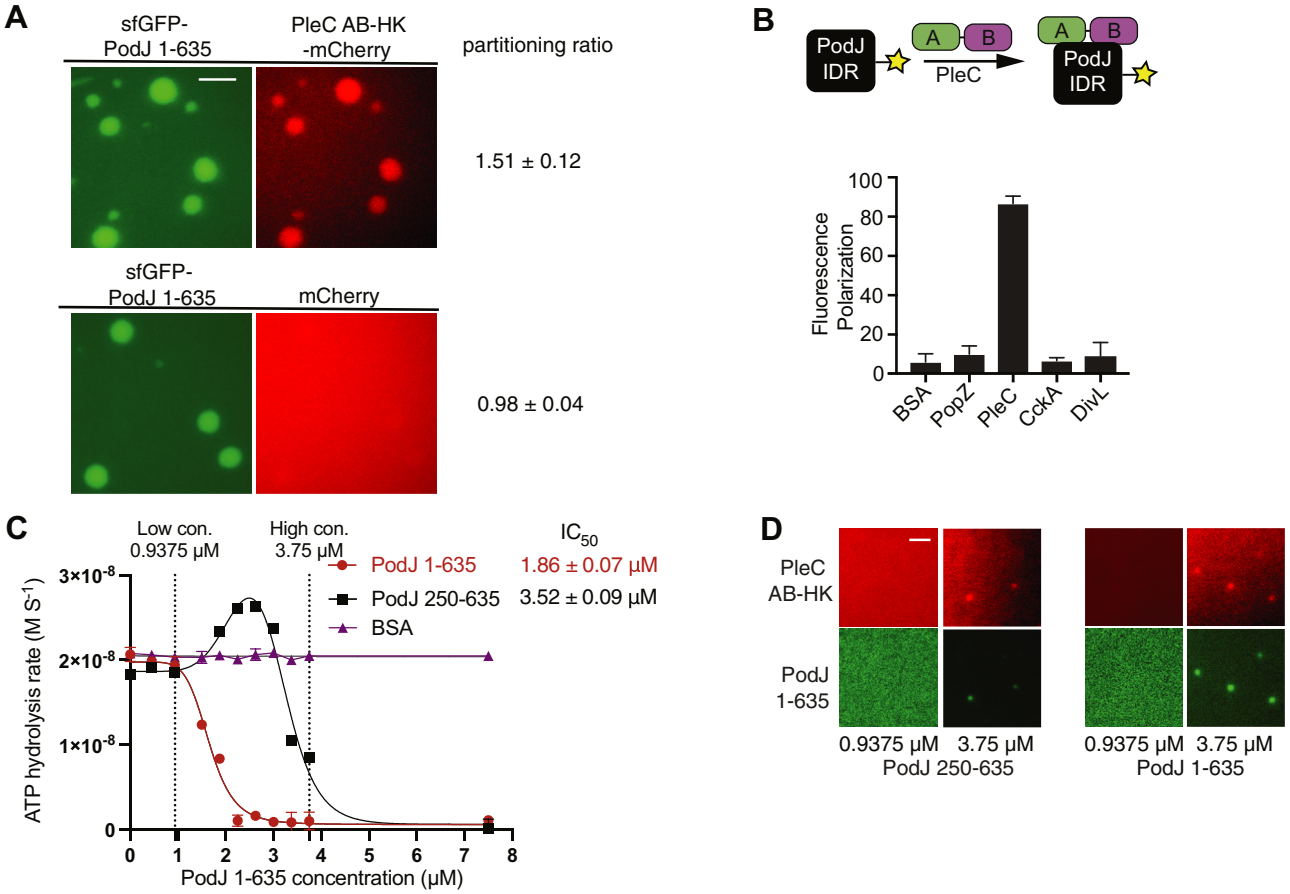

Figure 6. *In vitro* PodJ recruits PleC as a client and represses its kinase activity. *A*, fluorescence microscopy images of purified sfGFP-PodJ with PleC-mCherry. Purified proteins were mixed at 7.5 μM, 50 mM Tris-HCl pH 8.0, and 200 mM KCl. The scale bar represents 2.5 μm. *B*, fluorescence polarization binding assay of BODIPY dye-labeled 250 nM PodJ-IDR mixed with the following: 10 μM BSA, PopZ, PleC PAS-AB, CckA (70–691), or DivL (54–769). *C*, coupled enzyme assay measures the PodJ-activated activity switch of PleC. Conditions from *left* to *right*: 7.5 μM of PleC PAS AB-HK was incubated with 1 mM ATP and 0, 0.45, 0.9375, 1.875, 2.25, 2.625, 3, 3.375, 3.75, 7.5 μM of PodJ(1–635) (*red circle*), PodJ(250–635) (*black square*), or BSA (*purple triangle*), respectively. Data were fitted through nonlinear regression into [inhibitor] *versus* response for PodJ(1–635) and bell shaped for PodJ 250–635 using Prism 9. Error bars represent the standard deviation from two independent biological replicates. *D*, fluorescence microscopy images of kinase reaction mixtures containing purified sfGFP-PodJ(1–635) and sfGFP-PodJ(250–635) at 0.9375 and 3.75 μM. Purified proteins were mixed in kinase buffer supplemented with 1.0 mM ATP, 10 mM $MgCl_2$, 3 mM phosphoenolpyruvate, 0.2 mM NADH, 2 units of pyruvate kinase, and 6.6 units lactate dehydrogenase. The scale bar represents 2.5 μm.

Discussion

Reconstitution of the PodJ–PleC complex *in vitro* (Figs. 5 and 6) and in *E. coli* (Figs. 2–4) demonstrated that PodJ recruits and regulates PleC function through a PAS-IDR interaction. Our studies demonstrated that *in vitro* the PodJ–PleC phase separates as a biomolecular condensate. Therefore, we propose that the multivalency of PodJ, in conjunction with the PopZ scaffold (11, 12, 20), promotes phase separation of the new cell pole biomolecular condensate. Within this new cell pole biomolecular condensate, PodJ recruits and regulates PleC function at the cell poles. We showed that the N-terminal coiled coils were critical for cell pole accumulation of PodJ's cytoplasmic domains in *Caulobacter* and *E. coli* (Fig. 2*A*).

This study leveraged a truncation of PodJ, PodJ(1–635), that lacks the transmembrane tether. This truncation accumulates at the cell pole in *E. coli* and *C. crescentus* (Fig. 2*A*), recruits PleC to the cell poles (Fig. 2*B*), regulates PleC-CcaS function in *E. coli* (Fig. 3), and regulates PleC signaling *in vitro*. In addition, the PodJ(1–635) construct was accessible to protein purification, unlike $PodJ_S$ and $PodJ_L$. A drawback of the PodJ(1–635) truncation is that it is not the biologically relevant and membrane-associated form of $PodJ_S$ or $PodJ_L$. Unlike full-length PodJ, the IDR of PodJ(1–635) is no longer directly attached to the membrane and this surface may introduce nonnative interactions that influence phase separation.

Future development of purification strategies for the full-length membrane-associated PodJ will be needed for comparison. These studies will evaluate how PodJ's membrane tethering and its periplasmic domains impact PodJ phase separation and regulation of PleC signaling. Indeed, through PodJ truncation analysis in *C. crescentus*, Lawler *et al.* (30) have demonstrated that both the cytoplasmic and periplasmic domains of PodJ contribute to PodJ's ability to accumulate at the cell poles in *C. crescentus*. Moreover, additional studies are needed to conclude if full-length PodJ displays phase separation capabilities *in vivo* and if phase separation contributes to PodJ's ability to accumulate at the cell poles.

The discovery of PodJ's ability to directly regulate PleC function provides new data to understand how PodJ is logically connected to the cell cycle. Past work demonstrated that the

cell-cycle master regulators control PodJ's expression (49) and proteolysis once per cell cycle (31, 32). We observed that the shortened form of the PodJ scaffold retains the ability to recruit PleC to the cell poles. However, $PodJ_S$ no longer stimulates PleC-CcaS function. Thus, proteolytic remodeling of the PodJ within these new cell pole biomolecular condensates serves as a cell-cycle checkpoint signal to tune PleC function (Fig. 7).

Upon complete degradation of $PodJ_S$, PleC is liberated from the cell pole. In this diffuse state, PleC's activity is regulated by DivK allosteric stimulation (26) and pilus retraction (27). PleC kinase function stimulates downregulation of the CtrA pathway and the expression of new PodJ protein at the swarmer-to-stalk transition (49). This leads to stimulation of new cell pole localized PleC phosphatase function and activation of the CtrA pathway. Subsequently, robust activation of the downstream CtrA signaling pathway leads to the expression of PodJ-specific proteases (31, 32) that proteolyze $PodJ_L$ into $PodJ_S$. This proteolytic event tunes the functions of the PodJ biomolecular condensates resulting in phosphatase downregulation.

More broadly, phase separation provides an accessible compartmentalization strategy for the bacterial kingdom (7). The three scaffolding proteins, PopZ (11), SpmX (12), and PodJ (Figs. 4 and 5), phase separate as two distinct membraneless organelles at opposite ends of the cell. In addition, several other recent studies have shown that bacteria leverage phase separation to compartmentalize and regulate RNA polymerase (8), mRNA decay (9, 10), ABC transporters (13), DNA repair (14), cell division (15), chromosome segregation (17) and carboxysome assembly (19). These studies have laid the foundation to consider the extent and advantages of organizing biochemistry within biomolecular condensates in the bacterial cytoplasm.

Biomolecular condensates are generally thought to enhance enzyme reaction rates through mass action (50). Some recent studies have shown enhanced enzymatic rates, including RNA decapping (51), pyrenoid biochemistry (52) and SUMOylation (53). Here we have examined how biomolecular condensates regulate the histidine kinase activity of PleC. To determine the role of allostery, we found that a functional PAS sensor transmission motif was required for stimulation by full-length PodJ in *E. coli* (Fig. 4). This indicates that PodJ stimulation requires PleC-CcaS's sensor to kinase domain allosteric stimulation.

A comparison of PodJ-IDR or PodJΔCC1–3 *versus* full-length PodJ stimulation of our *in vivo* PleC-CcaS reporter revealed a 3-fold *versus* 10-fold degree of stimulation. Given that neither PodJ-IDR nor PodJΔCC1–3 accumulated as a focus, this indicates that PodJ ability to bind to PleC in the dilute phase can regulate PleC-CcaS function. In contrast, the full-length PodJ variant that accumulates at the cell poles leads to an additional 3.3-fold activation of PleC-CcaS (Fig. 3). Comparison of PodJ–PleC constructs that exist solely in the dilute phase *versus* PodJ–PleC constructs that exist primarily in the protein-rich phase suggests that the contributions from mass action and the unique chemical environment contribute an additional 3.3-fold to PleC's activity *in vivo*.

Similarly, we observed that PodJ (1–635) could repress the activity of PleC *in vitro* under conditions where phase separation readily occurred (Fig. 6, *C* and *D*). In both cases, we suspect that there are interconnected contributions from mass action and kinase allostery. The localized high concentration of PodJ–PleC may promote an active PodJ–PleC conformation

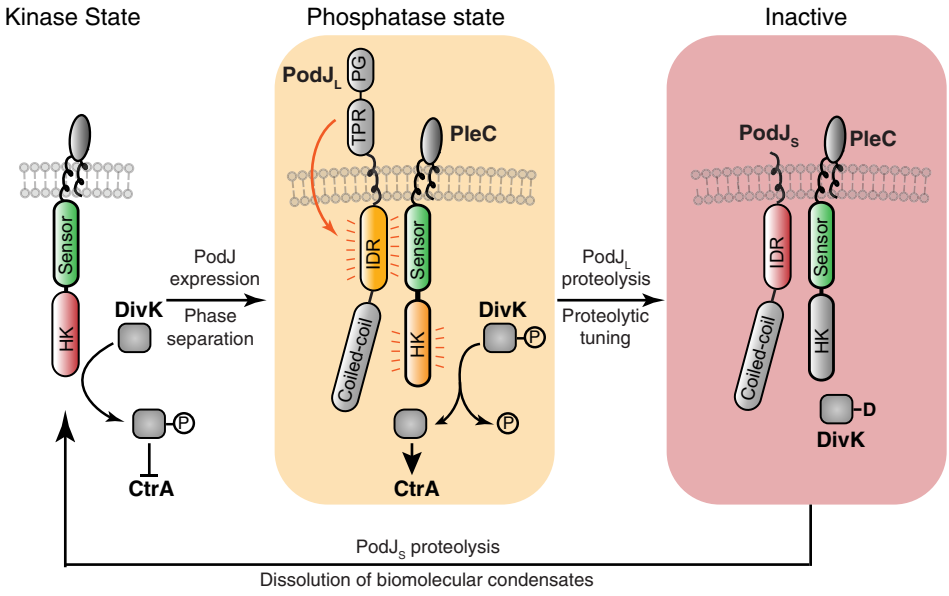

Figure 7. Proposed model for cell-cycle–dependent phase separation, proteolytic tuning of biochemical function, and dissolution of a biomolecular condensate that regulates a histidine kinase. PodJ serves as a cell-cycle checkpoint signal that regulates the formation and activity of PodJ–PleC biomolecular condensate. PleC alone can function as a kinase, which leads to inhibition of the CtrA pathway and expression of $PodJ_L$. The cell pole–localized $PodJ_L$–PleC complex represses PleC kinase activity. This leads to CtrA pathway activation and the expression of PodJ proteases. Proteolysis of $PodJ_L$ to its short form $PodJ_S$ leads to an inactive form of PleC that may have kinase functions. Proteolysis of $PodJ_S$ leads to the dissolution of the PodJ–PleC biomolecular condensate and liberates PleC from the cell pole. For simplicity of illustration, PleC naturally exists as a dimer but is depicted as a monomer.

in contrast to the lower PodJ–PleC concentration in the dilute phase. Similarly, it was shown that phase separation of the *Saccharomyces cerevisiae* RNA decapping complex Dcp1/Dcp2 was coupled to conformational control of RNA decapping enzymatic activity (51).

Two other histidine kinases, CckA (24) and DivJ (12), also show activation of enzyme function at high packing density on liposomes. In addition, both PleC and CckA require their N-terminal PAS sensory domain to mediate enzyme regulation at increased local concentration. Collectively these three studies suggest that strategies that concentrate histidine kinases, such as phase separation, may have a common effect of robustly stimulating low-copy histidine kinases (12, 24). More broadly, the coupling of conformational change to the increased enzyme concentration (51) in biomolecular condensates may present a generalizable way to regulate enzyme function.

In summary, two-component systems provide bacterial cells with a customizable signaling platform. PleC has been customized for spatial control through phase separation and temporal control through sensing the cell-cycle produced and degraded signal PodJ. Moreover, PleC integrates both intra- and extracellular signals (27) to coordinate growth and development. Therefore, the interplay of scaffolds, phase separation, and two-component systems provide avenues to orchestrate bacteria's complex development.

Experimental procedures

Bacterial strains

All experiments were performed using *C. crescentus* NA1000 (also known as CB15N) and *E. coli* DH5α and BL21 purchased from Promega. *C. crescentus* NA1000 was a kind gift from Dr Lucy Shapiro (Stanford University School of Medicine). PCR reactions and primers used for Gibson assembly are listed in Table S1. All relevant primers are given in detail in Table S2. Plasmids used in this study are listed in Table S3. More strains are listed in Table S4. Transformations were carried out as described (54). Details about plasmid and strain construction are listed in Text S1.

Plasmid cloning strategies

Fragments of target genes plasmid backbone were amplified *via* PCR using Phusion polymerase (Thermo Scientific). PCR reactions were performed in 50 μl reaction mixtures containing 3% (v/v) dimethyl sulfoxide, 1.3 M betaine, 0.3 μM each primer, 0.2 mM each dNTP, and 1 U Phusion High-Fidelity DNA Polymerase (Thermo Scientific). Both fragments were purified *via* gel extraction. Gibson assembly (55) reactions were performed in 20 μl with 100 ng backbone and typically a 1:10 backbone:insert ratio. A Gibson reaction master mix was prepared from 5x reaction buffer, T5 exonuclease (NEB), Phusion polymerase (NEB), Taq ligase (NEB) and stored as aliquots of 15 μl at −20 °C. An annealing temperature of 55 °C was used for all reactions, followed by 10 min at 4 °C, and 10 μl of the reaction product was then transformed into chemically competent *E. coli* DH5a cells using the KCM transformation method. Oligonucleotide primers applied for amplification of the gene insert were designed using the j5 online program, and they featured overlaps of 26 bases to the insertion site in the plasmid (56). Oligonucleotides were synthesized by IDT, and all DNA sequencing reactions were performed by Genewiz. DNA oligos, plasmid construction methods, plasmids, and strains used in this study are listed in Tables S1–S4. Plasmids containing the CcaS-CcaR green light sensing system pJT119b was a gift from Jeffrey Tabor (Addgene plasmid # 50551; http://n2t.net/addgene:50551; RRID:Addgene_50551).

Growth and induction conditions

C. crescentus strains were grown at 28 °C in peptone yeast extract. *E. coli* strains used for protein purifications and microscopy experiments were grown at 37 °C in LB medium unless otherwise stated. When required, protein expression was induced by adding 0.002 to 0.5 mM isopropyl β-D-1-thiogalactopyranoside (IPTG) or 0.5 to 10 mM arabinose in *E. coli* and 0.003% to 0.3% xylose or 0.005 to 0.5 mM vanillic acid in *C. crescentus* unless otherwise stated. The induction time for microscopy experiments is 0.5 to 2 h in *E. coli* and 3 to 5 h in *C. crescentus*.

Phase contrast and epifluorescence microscopy

Cells were imaged after being immobilized on a 1.5% w/v agarose/media (peptone yeast extract for *C. crescentus* and LB for *E. coli*) pad. Phase microscopy was performed by a Nikon Eclipse T*i*-E inverted microscope equipped with an Andor Ixon Ultra DU897 EMCCD camera and a Nikon CFI Plan-Apochromat 100X/1.45 oil objective. The excitation source was a Lumencor SpectraX light engine. Chroma filter cube CFP/YFP/MCHRY MTD TI was used to image ECFP (465/25M), EYFP (545/30M), and mCherry (630/60M). Chroma filter cube DAPI/GFP/TRITC was used to image sfGFP (515/30M). Images were collected and processed with Nikon NIS-Elements AR software, ImageJ (57), and MicrobeJ (58).

Protein expression and purification of PodJ, PopZ, PleC, CckA, and DivL

Protein expression for PodJ, PopZ, PleC, and CckA followed the same protocol described in detail below for PodJ(1–635). To purify the cytoplasmic portion of PodJ(1–635), Rosetta (DE3) containing plasmid pwz091 was grown in 6 L LB medium (30 μg/ml chloramphenicol and 100 μg/ml ampicillin) at 37 °C. The culture was then induced at an A_{600} of 0.4 to 0.6 with 0.5 mM IPTG overnight at 18 °C. The cells were harvested and resuspended in the lysis buffer (50 mM Tris-HCl, 700 mM KCl, 20 mM Imidazole, 0.05% dextran sulfate, pH 8.0) in the presence of protease inhibitor cocktail tablets without EDTA (Roche). The cell suspension was lysed with three passes through an EmulsiFlex-C5 cell disruptor (AVESTIN, Inc), and the supernatant was collected by centrifuging at 12,000*g* for 30 min at 4 °C. In addition, the insoluble cell debris was resuspended by the recovery buffer (50 mM Tris-HCl, 1000 mM KCl, 20 mM Imidazole, 0.05% dextran sulfate, pH 8.0), and its supernatant was collected as well as the previous centrifugation. The combined supernatants were loaded onto a

5-ml HisTrap HP column (GE Healthcare) and purified with the ÄKTA FPLC System. After washing with 10 volumes of wash buffer (50 mM Tris-HCl, 300 mM KCl, and 25 mM imidazole, pH 8.0), the protein was collected by elution from the system with elution buffer (50 mM Tris-HCl, 300 mM KCl, and 500 mM imidazole, pH 8.0). Then the protein was concentrated to a 3 ml volume using Amicon Centrifugal Filter Units, resulting in over 95% purity. Then the protein was dialyzed with a buffer containing 50 mM Tris-HCl (pH 8.0), 300 mM KCl and then aliquoted to a small volume (100 µl) and kept frozen at −80 °C until use.

Labeling of SNAP-PodJ(1–635) with SNAP-Cell 505-Star

SNAP-PodJ(1–635) was purified by following the protocol described above until the FPLC purification and Amicon centrifuge concentration step. Then the protein in the wash buffer was incubated with SNAP-Cell 505-Star in a 1:1.2 molar ratio at 0 °C for 3 h. Next, the mixture was dialyzed against a dialysis buffer containing 50 mM Tris-HCl (pH 8.0), 300 mM KCl, then aliquoted to a small volume (20 µl) and kept frozen at −80 °C until ready to use for imaging.

Fluorescence polarization assay

To label PodJ-IDR (471–635), we cloned a cysteine just after the 6X-His-tag proteins at the N terminus of each protein. Cys-PodJ-IDR expression and purification followed the same protocol as PodJ mentioned above. These two proteins were labeled at the cysteine using thiol-reactive BODIPY FL N-(2-Aminoethyl) Maleimide (Thermo Fisher). The proteins were mixed with 10-fold excess BODIPY FL N-(2-Aminoethyl) Maleimide and allowed to react for 2 h at room temperature. The unreacted dye was quenched with mercaptoethanol (5% final concentration). The labeled proteins were purified *via* dialysis to remove unreacted fluorescent dye (5 times, 500 ml buffer, and 30 min each).

Fluorescence polarization binding assays were performed by mixing 100 nM labeled proteins with 0, 0.25, 0.5, 1, 2, 4, 8, 16 µM partner protein (PopZ, CckA, PleC, DivL, or BSA) for 45 min to reach binding equilibrium at the room temperature. Fluorescent proteins were excited at 470 nm, and emission polarization was measured at 530 nm in a UV-visible Evol 600 spectrophotometer (Thermo Fisher). Fluorescent polarization measurements were performed in triplicates, and three independent trials were averaged with error bars representing the standard deviation.

Quantification and statistical analysis

FIJI/ImageJ (57) and MicrobeJ (58) were used for image analysis. More than 100 representative droplets were selected for partitioning ratio calculation, and each droplet's fluorescent intensity inside was divided by the background intensity outside. The mean and standard deviation for each measurement is shown. The number of replicates and the number of cells analyzed per replicate is specified in corresponding legends. All experiments were replicated three times, and statistical comparisons were carried out using GraphPad Prism with two-tailed Student's *t* tests. Differences were significant when *p* values were below 0.05. In all figures, measurements are shown as mean ± standard deviation (SD).

Fluorescence microscopy imaging of biomolecular condensates

sfGFP-PodJ(1–635), PleC PAS AB-HK-mCherry, SNAP-PodJ(1–635), sfGFP, mCherry protein aliquots were thawed on ice along with KCl, Tris-HCl (pH=8.0), 1,6-hexanediol, ATP, ADP, and sterile water. Working solutions of protein, Tris-HCl (pH=8.0), and KCl were combined, diluted with water to various concentrations, and incubated at room temperature for 15 min before imaging. Then the incubated sample mix was pipetted onto the slides with SureSeal Imaging Spacers (Electron Microscopy Sciences) and covered with coverslips (VWR). All images were taken with an Eclipse Ti-E inverted microscope (Nikon) in both phase-contrast and fluorescent channels using a Plan Apo 100x objective.

Size exclusion chromatography and native gel analysis

A gel filtration standard (Sigma) containing thyroglobulin (bovine, 669 kDa), carbonic anhydrase (bovine, 29 kDa), blue dextran (2000 kDa), apoferritin (horse, 443 kDa), β-Amylase (sweet potato, 200 kDa), alcohol dehydrogenase (yeast, 150 kDa), and albumin (bovine, 66 kDa) was used to generate a molecular weight standard plot using a Superdex 200 10/300 GL column (GE Healthcare). A 3.2-mg/ml sample of His-PodJ(1–635) in a buffer containing 50 mM Tris-HCl (pH 8.0), 300 mM KCl was loaded onto the gel filtration column. Samples eluted after 7.9, 12.8, and 15.0 ml of elution buffer corresponding to a molecular weight of 1851, 194, and 70.7 kDa (theoretical monomer = 73.0 kDa). One representative result of triplicates was shown.

His-PodJ(1–635) was also analyzed by running a native gel. Protein was separated by gel electrophoresis (8% resolving gel) at 80 V for 4 h at 4 °C, using a native protein ladder (range from 66 to 669 kDa, Thermo Fisher).

Western blotting

We analyzed protein levels and potential proteolysis for each protein construct expression in *E. coli* and *C. crescentus* through Western blot analysis. These assays indicated that each PodJ and PleC variant was expressed and exhibited little to no proteolysis (Fig. S10). For the Western blotting, log-phase cells were induced with 0.002 to 0.5 mM isopropyl β-D-1-thiogalactopyranoside (IPTG) or 0.5 to 10 mM arabinose in *E. coli* for 0.5 to 2 h, and 0.003% to 0.3% xylose or 0.005 to 0.5 mM vanillic acid in *C. crescentus* for 3 to 5 h unless otherwise stated. After induction was complete, the cells were pelleted and resuspended in 250 ml of 2x Laemmli buffer for each 1.0 A_{600} unit. The samples were boiled at 95 °C for 10 min, then vortexed. Next, 10 µl of samples was loaded in a 10% SDS-PAGE gel and run at 125 V for 90 min. Then the transfer was done at 20 V for 80 min at 0 °C. Blocking was done for 1 h using 25 ml of blocking buffer (25 ml 1x TBST, 1.25 g nonfat dry milk) at 0 °C with gentle shaking. For primary antibody blotting, the membrane was submerged in

1:5000 dilution of the anti-GFP (#2956S, Cell Signaling) or anti-mCherry (#43590S, Cell Signaling) antibody in the buffer (10 ml 1x TBST, 0.5 g BSA, 10 μl antibody) and shacken gently for 1 h at room temperature. After washing the membrane 3 times with 1x TBST for 5 min each, the membrane was incubated with secondary antibody (1:10,000) anti-goat IgG secondary antibody (A0545, Sigma Aldrich) in the buffer (10 ml 1x TBST, 0.5 g nonfat dry milk, 1 μl antibody) for 1 h with gentle shaking at room temperature. Next, the membrane was washed 3 times, 5 min each, with 1x TBST buffer with gentle shaking. After the wash, the membrane was placed in Pierce chemiluminescence substrates for 5 min and imaged on film using ChemiDoc (Bio-Rad).

PleC-CcaS chimera reporter assay

PleC-CcaS chimera reporter assays were performed based on the following steps. Starting from a −80 °C dimethyl sulfoxide freezer stock, strains were inoculated into 5 ml LB Miller Broth in culture tubes containing appropriate antibiotics and grown at 37 °C 220 rpm for overnight. Cultures were then diluted with fresh and sterile LB media to A_{600} =1.0 using a UV-visible spectrophotometer (VWR). The cells were then inoculated into fresh LB media with a density of 25 μl per 1 ml LB media with appropriate antibiotics. The tubes were shaken at 37 °C 220 rpm until A_{600} reached 0.4. Then PodJ was induced with 5 mM arabinose for another 4 h. After that, cells were transferred into 96-well plates. Fluorescence was measured using a 5 nm bandpass with excitation/emission for mCherry (585/nm/610 nm)/CFP (456 nm/480 nm)/YFP (513 nm/527 nm) with a manually set gain of 50. Each construct was repeated with three independent biological replicates as indicated in the standard error in the bar graph.

Homology modeling

The PleC protein sequence was submitted into HHpred to predict protein features, fetch published crystal structures as templates and generate multiple sequences alignment (59). A template (PDB:4GCZ) was selected to model the homology structure of PleC PAS-A and PAS-B, respectively. Homology models were then downloaded and edited with PyMol to highlight secondary structures and signal transmission motif DI/VT residues at the C terminus of each PAS domain.

Coupled enzyme activity assay

Kinase activity was measured using a coupled enzyme assay (44). Purified proteins, 7.5 μM, were mixed in kinase buffer supplemented with 1.0 mM ATP, 10 mM $MgCl_2$, 3 mM phosphoenolpyruvate, 0.2 mM NADH, 2 units of pyruvate kinase, and 6.6 units of lactate dehydrogenase (P0294, Sigma). Reactions were performed in three replicates in a 100 μl volume and loaded into a clear polystyrene 384-well plate. Each reaction was initiated by adding ATP, and 340 nm absorbance was recorded every 10 s for 90 min on a Tecan M1000 microplate reader (Tecan). The slope of a stable, linear absorbance decay was measured to calculate ATP hydrolysis rates (60). Background rates of ATP hydrolysis and NADH oxidation were measured and subtracted from observed ATP hydrolysis rates without adding any protein. The mean observed rate and SD were determined and analyzed using Prism (GraphPad).

Data availability

The authors declare that the data supporting the findings of the study are available within this article and its Supplementary Information Files or from the corresponding author (W. S. C.). In addition, the plasmids and strains used in this study are available from the corresponding author (W. S. C.) upon request.

Supporting information—This article contains supporting information (3, 30, 55, 56, 61-67).

Acknowledgments—We thank the Lucy Shapiro lab at Stanford University for providing the NA1000 strain used in this study. We thank Dylan Tomares and Jiefei Wang from Childers laboratory for their critiques on the experiments and writing. We thank Saumya Saurabh and Jared Schrader for discussions on biomolecular condensates in bacteria. We thank the Alex Deiters lab at the University of Pittsburgh for sharing the Tecan 100 plate reader that supported measurements in this study.

Author contributions—W. S. C., W. Z., and C. Z. conceptualization; W. S. C., W. Z., and C. Z. methodology; C. Z. and W. Z. formal analysis; W. Z., K. A. K., C. Z., S. W. D., and W. S. C. investigation; W. S. C. resources; W. S. C. data curation; W. S. C. and C. Z. writing – original draft; W. Z., S. W. D., and K. A. K. writing – review & editing; W. S. C. supervision; W. S. C. project administration; W. S. C. funding acquisition.

Funding and additional information—This research was funded through the University of Pittsburgh Start-up funds to W. S. C.

Conflict of interest—The authors declare that they have no conflicts of interest with the contents of this article.

Abbreviations—The abbreviations used are: BSA, bovine serum albumin; IDR, intrinsically disordered region; TM, transmembrane.

References

1. Smock, R. G., and Gierasch, L. M. (2009) Sending signals dynamically. *Science* **324**, 198–203
2. Bhattacharyya, R. P., Remenyi, A., Good, M. C., Bashor, C. J., Falick, A. M., and Lim, W. A. (2006) The Ste5 scaffold allosterically modulates signaling output of the yeast mating pathway. *Science* **311**, 822–826
3. Banani, S. F., Lee, H. O., Hyman, A. A., and Rosen, M. K. (2017) Biomolecular condensates: Organizers of cellular biochemistry. *Nat. Rev. Mol. Cell Biol.* **18**, 285–298
4. Cohan, M. C., and Pappu, R. V. (2020) Making the case for disordered proteins and biomolecular condensates in bacteria. *Trends Biochem. Sci.* **45**, 668–680
5. Brangwynne, C. P. (2013) Phase transitions and size scaling of membraneless organelles. *J. Cell Biol.* **203**, 875–881
6. Fare, C. M., Villani, A., Drake, L. E., and Shorter, J. (2021) Higher-order organization of biomolecular condensates. *Open Biol.* **11**, 210137
7. Azaldegui, C. A., Vecchiarelli, A. G., and Biteen, J. S. (2021) The emergence of phase separation as an organizing principle in bacteria. *Biophys. J.* **120**, 1123–1138

8. Ladouceur, A.-M., Parmar, B. S., Biedzinski, S., Wall, J., Tope, S. G., Cohn, D., Kim, A., Soubry, N., Reyes-Lamothe, R., and Weber, S. C. (2020) Clusters of bacterial RNA polymerase are biomolecular condensates that assemble through liquid–liquid phase separation. *Proc. Natl. Acad. Sci. U. S. A.* **117**, 18540–18549
9. Al-Husini, N., Tomares, D. T., Childers, W. S., and Schrader, J. (2018) α-Proteobacterial RNA degradosomes assemble liquid-liquid phase separated RNP bodies. *Mol. Cell* **71**, 1027–1039.e14
10. Al-Husini, N., Tomares, D. T., Pfaffenberger, Z. J., Muthunayake, N. S., Samad, M. A., Zuo, T., Bitar, O., Aretakis, J. R., Bharmal, M. M., Gega, A., Biteen, J. S., Childers, W. S., and Schrader, J. M. (2020) BR-bodies provide selectively permeable condensates that stimulate mRNA decay and prevent release of decay intermediates. *Mol. Cell* **78**, 670–682.e8
11. Lasker, K., von Diezmann, L., Zhou, X., Ahrens, D. G., Mann, T. H., Moerner, W. E., and Shapiro, L. (2020) Selective sequestration of signalling proteins in a membraneless organelle reinforces the spatial regulation of asymmetry in Caulobacter crescentus. *Nat. Microbiol.* **5**, 418–429
12. Saurabh, S., Chong, T. N., Bayas, C., Dahlberg, P. D., Cartwright, H. N., Moerner, W. E., and Shapiro, L. (2022) ATP-responsive biomolecular condensates tune bacterial kinase signaling. *Sci. Adv.* **8**, eabm6570
13. Heinkel, F., Abraham, L., Ko, M., Chao, J., Bach, H., Hui, L. T., Li, H., Zhu, M., Ling, Y. M., Rogalski, J. C., Scurll, J., Bui, J. M., Mayor, T., Gold, M. R., Chou, K. C., *et al.* (2019) Phase separation and clustering of an ABC transporter in Mycobacterium tuberculosis. *Proc. Natl. Acad. Sci. U. S. A.* **116**, 16326–16331
14. Harami, G. M., Kovács, Z. J., Pancsa, R., Pálinkás, J., Baráth, V., Tárnok, K., Málnási-Csizmadia, A., and Kovács, M. (2020) Phase separation by ssDNA binding protein controlled *via* protein–protein and protein–DNA interactions. *Proc. Natl. Acad. Sci. U. S. A.* **117**, 26206–26217
15. Monterroso, B., Zorrilla, S., Sobrinos-Sanguino, M., Robles-Ramos, M. A., Lopez-Alvarez, M., Margolin, W., Keating, C. D., and Rivas, G. (2019) Bacterial FtsZ protein forms phase-separated condensates with its nucleoid-associated inhibitor SlmA. *EMBO Rep.* **20**, e45946
16. Robles-Ramos, M.Á., Zorrilla, S., Alfonso, C., Margolin, W., Rivas, G., and Monterroso, B. (2021) Assembly of bacterial cell division protein FtsZ into dynamic biomolecular condensates. *Biochim. Biophys. Acta Mol. Cell Res.* **1868**, 118986
17. Guilhas, B., Walter, J.-C., Rech, J., David, G., Walliser, N. O., Palmeri, J., Mathieu-Demaziere, C., Parmeggiani, A., Bouet, J.-Y., Le Gall, A., and Nollmann, M. (2020) ATP-driven separation of liquid phase condensates in bacteria. *Mol. Cell* **79**, 293–303.e294
18. Pattanayak, G. K., Liao, Y., Wallace, E. W. J., Budnik, B., Drummond, D. A., and Rust, M. J. (2020) Daily cycles of reversible protein condensation in cyanobacteria. *Cell Rep.* **32**, 108032
19. MacCready, J. S., Basalla, J. L., and Vecchiarelli, A. G. (2020) Origin and evolution of carboxysome positioning systems in cyanobacteria. *Mol. Biol. Evol.* **37**, 1434–1451
20. Holmes, J. A., Follett, S. E., Wang, H., Meadows, C. P., Varga, K., and Bowman, G. R. (2016) Caulobacter PopZ forms an intrinsically disordered hub in organizing bacterial cell poles. *Proc. Natl. Acad. Sci. U. S. A.* **113**, 12490–12495
21. Perez, A. M., Mann, T. H., Lasker, K., Ahrens, D. G., Eckart, M. R., and Shapiro, L. (2017) A localized complex of two protein oligomers controls the orientation of cell polarity. *mBio* **8**, e02238-16
22. Hinz, A. J., Larson, D. E., Smith, C. S., and Brun, Y. V. (2003) The Caulobacter crescentus polar organelle development protein PodJ is differentially localized and is required for polar targeting of the PleC development regulator. *Mol. Microbiol.* **47**, 929–941
23. Curtis, P. D., Quardokus, E. M., Lawler, M. L., Guo, X., Klein, D., Chen, J. C., Arnold, R. J., and Brun, Y. V. (2012) The scaffolding and signalling functions of a localization factor impact polar development. *Mol. Microbiol.* **84**, 712–735
24. Mann, T. H., Seth Childers, W., Blair, J. A., Eckart, M. R., and Shapiro, L. (2016) A cell cycle kinase with tandem sensory PAS domains integrates cell fate cues. *Nat. Commun.* **7**, 11454
25. Mann, T. H., and Shapiro, L. (2018) Integration of cell cycle signals by multi-PAS domain kinases. *Proc. Natl. Acad. Sci. U. S. A.* **115**, E7166–e7173
26. Paul, R., Jaeger, T., Abel, S., Wiederkehr, I., Folcher, M., Biondi, E. G., Laub, M. T., and Jenal, U. (2008) Allosteric regulation of histidine kinases by their cognate response regulator determines cell fate. *Cell* **133**, 452–461
27. Del Medico, L., Cerletti, D., Schachle, P., Christen, M., and Christen, B. (2020) The type IV pilin PilA couples surface attachment and cell-cycle initiation in Caulobacter crescentus. *Proc. Natl. Acad. Sci. U. S. A.* **117**, 9546–9553
28. Wheeler, R. T., and Shapiro, L. (1999) Differential localization of two histidine kinases controlling bacterial cell differentiation. *Mol. Cell* **4**, 683–694
29. Viollier, P. H., Sternheim, N., and Shapiro, L. (2002) Identification of a localization factor for the polar positioning of bacterial structural and regulatory proteins. *Proc. Natl. Acad. Sci. U. S. A.* **99**, 13831–13836
30. Lawler, M. L., Larson, D. E., Hinz, A. J., Klein, D., and Brun, Y. V. (2006) Dissection of functional domains of the polar localization factor PodJ in Caulobacter crescentus. *Mol. Microbiol.* **59**, 301–316
31. Chen, J. C., Hottes, A. K., McAdams, H. H., McGrath, P. T., Viollier, P. H., and Shapiro, L. (2006) Cytokinesis signals truncation of the PodJ polarity factor by a cell cycle-regulated protease. *EMBO J.* **25**, 377–386
32. Chen, J. C., Viollier, P. H., and Shapiro, L. (2005) A membrane metalloprotease participates in the sequential degradation of a Caulobacter polarity determinant. *Mol. Microbiol.* **55**, 1085–1103
33. Brilli, M., Fondi, M., Fani, R., Mengoni, A., Ferri, L., Bazzicalupo, M., and Biondi, E. G. (2010) The diversity and evolution of cell cycle regulation in alpha-proteobacteria: A comparative genomic analysis. *BMC Syst. Biol.* **4**, 52
34. Ebersbach, G., Briegel, A., Jensen, G. J., and Jacobs-Wagner, C. (2008) A self-associating protein critical for chromosome attachment, division, and polar organization in Caulobacter. *Cell* **134**, 956–968
35. Levskaya, A., Chevalier, A. A., Tabor, J. J., Simpson, Z. B., Lavery, L. A., Levy, M., Davidson, E. A., Scouras, A., Ellington, A. D., Marcotte, E. M., and Voigt, C. A. (2005) Synthetic biology: Engineering *Escherichia coli* to see light. *Nature* **438**, 441–442
36. Wang, J., Zhang, C., and Childers, W. S. (2021) A biosensor for detection of indole metabolites. *ACS Synth. Biol.* **10**, 1605–1614
37. Olson, E. J., Hartsough, L. A., Landry, B. P., Shroff, R., and Tabor, J. J. (2014) Characterizing bacterial gene circuit dynamics with optically programmed gene expression signals. *Nat Methods* **11**, 449
38. Diensthuber, R. P., Bommer, M., Gleichmann, T., and Moglich, A. (2013) Full-length structure of a sensor histidine kinase pinpoints coaxial coiled coils as signal transducers and modulators. *Structure* **21**, 1127–1136
39. Moglich, A., Ayers, R. A., and Moffat, K. (2009) Structure and signaling mechanism of Per-ARNT-Sim domains. *Structure* **17**, 1282–1294
40. Aretakis James, R., Gega, A., Schrader Jared, M., and Arumugam, M. (2019) Absolute measurements of mRNA translation in Caulobacter crescentus reveal important fitness costs of vitamin B12 scavenging. *mSystems* **4**, e00170-19
41. Molliex, A., Temirov, J., Lee, J., Coughlin, M., Kanagaraj, A. P., Kim, H. J., Mittag, T., and Taylor, J. P. (2015) Phase separation by low complexity domains promotes stress granule assembly and drives pathological fibrillization. *Cell* **163**, 123–133
42. Patel, A., Malinovska, L., Saha, S., Wang, J., Alberti, S., Krishnan, Y., and Hyman, A. A. (2017) ATP as a biological hydrotrope. *Science* **356**, 753
43. Mehringer, J., Do, T.-M., Touraud, D., Hohenschutz, M., Khoshsima, A., Horinek, D., and Kunz, W. (2021) Hofmeister *versus* Neuberg: Is ATP really a biological hydrotrope? *Cell Rep. Phys. Sci.* **2**, 100343
44. Blair, J. A., Xu, Q., Childers, W. S., Mathews, I. I., Kern, J. W., Eckart, M., Deacon, A. M., and Shapiro, L. (2013) Branched signal wiring of an essential bacterial cell-cycle phosphotransfer protein. *Structure* **21**, 1590–1601
45. Buschiazzo, A., and Trajtenberg, F. (2019) Two-component sensing and regulation: How do histidine kinases talk with response regulators at the molecular level? *Annu. Rev. Microbiol.* **73**, 507–528

46. Albanesi, D., Martín, M., Trajtenberg, F., Mansilla, M. A. C., Haouz, A., Alzari, P. M., de Mendoza, D., and Buschiazzo, A. (2009) Structural plasticity and catalysis regulation of a thermosensor histidine kinase. *Proc. Natl. Acad. Sci. U. S. A.* **106**, 16185–16190
47. Gasser, C., Taiber, S., Yeh, C. M., Wittig, C. H., Hegemann, P., Ryu, S., Wunder, F., and Moglich, A. (2014) Engineering of a red-light-activated human cAMP/cGMP-specific phosphodiesterase. *Proc. Natl. Acad. Sci. U. S. A.* **111**, 8803–8808
48. Nakajima, M., Ferri, S., Rogner, M., and Sode, K. (2016) Construction of a miniaturized chromatic acclimation sensor from cyanobacteria with reversed response to a light signal. *Sci. Rep.* **6**, 37595
49. Crymes, W. B., Jr., Zhang, D., and Ely, B. (1999) Regulation of podJ expression during the Caulobacter crescentus cell cycle. *J. Bacteriol.* **181**, 3967–3973
50. Lyon, A. S., Peeples, W. B., and Rosen, M. K. (2021) A framework for understanding the functions of biomolecular condensates across scales. *Nat. Rev. Mol. Cell Biol.* **22**, 215–235
51. Tibble, R. W., Depaix, A., Kowalska, J., Jemielity, J., and Gross, J. D. (2021) Biomolecular condensates amplify mRNA decapping by biasing enzyme conformation. *Nat. Chem. Biol.* **17**, 615–623
52. Wunder, T., Cheng, S. L. H., Lai, S.-K., Li, H.-Y., and Mueller-Cajar, O. (2018) The phase separation underlying the pyrenoid-based microalgal Rubisco supercharger. *Nat. Commun.* **9**, 5076
53. Peeples, W., and Rosen, M. K. (2021) Mechanistic dissection of increased enzymatic rate in a phase-separated compartment. *Nat. Chem. Biol.* **17**, 693–702
54. Ely, B. (1991) Genetics of Caulobacter crescentus. *Methods Enzymol.* **204**, 372–384
55. Gibson, D. G., Young, L., Chuang, R. Y., Venter, J. C., Hutchison, C. A., 3rd, and Smith, H. O. (2009) Enzymatic assembly of DNA molecules up to several hundred kilobases. *Nat. Methods* **6**, 343–345
56. Hillson, N. J., Rosengarten, R. D., and Keasling, J. D. (2012) j5 DNA assembly design automation software. *ACS Synth. Biol.* **1**, 14–21
57. Schneider, C. A., Rasband, W. S., and Eliceiri, K. W. (2012) NIH image to ImageJ: 25 years of image analysis. *Nat. Methods* **9**, 671–675
58. Ducret, A., Quardokus, E. M., and Brun, Y. V. (2016) MicrobeJ, a tool for high throughput bacterial cell detection and quantitative analysis. *Nat. Microbiol.* **1**, 16077
59. Zimmermann, L., Stephens, A., Nam, S. Z., Rau, D., Kubler, J., Lozajic, M., Gabler, F., Soding, J., Lupas, A. N., and Alva, V. (2018) A completely reimplemented MPI bioinformatics toolkit with a new HHpred server at its core. *J. Mol. Biol.* **430**, 2237–2243
60. Kiianitsa, K., Solinger, J. A., and Heyer, W. D. (2003) NADH-coupled microplate photometric assay for kinetic studies of ATP-hydrolyzing enzymes with low and high specific activities. *Anal. Biochem.* **321**, 266–271
61. Jones, D. T. (1999) Protein secondary structure prediction based on position-specific scoring matrices. *J. Mol. Biol.* **292**, 195–202
62. Fiser, A., and Sali, A. (2003) Modeller: generation and refinement of homology-based protein structure models. *Methods Enzymol.* **374**, 461–491
63. Emenecker, R. J., Griffith, D., and Holehouse, A. S. (2021) Metapredict: a fast, accurate, and easyto- use cross-platform predictor of consensus disorder. *bioRxiv*, 2021.05.30.446349
64. The UniProt Consortium (2021) UniProt: the universal protein knowledgebase in 2021. *Nucleic Acids Res.* **49**, D480–D489
65. Hofmann, K., and Stoffel, W. (1993) TMbase-a database of membrane spanning proteins segments. *Biol. Chem. Hoppe Seyler* **347**, 166
66. Rice, P., Longden, I., and Bleasby, A. (2000) EMBOSS: the European Molecular Biology Open Software Suite. *Trends Genet.* **16**, 276–277
67. Crooks, G. E., Hon, G., Chandonia, J. M., and Brenner, S. E. (2004) WebLogo: a sequence logo generator. *Genome Res.* **14**, 1188–1190

ASBMB